Table 3 Summary of simulation for CBF and OEF in the case '25%' and the case '100%' of normal model using the DARG method with the subtraction method

$CO–O_2$ time lag (s)	CBF			OEF		
	Average (mL/g/min)	Error (%)	COV (%)	Average	Error (%)	COV (%)
Case '25%'						
60	0.50	0.15	0.37	0.40	−0.17	0.54
100	0.50	0.16	0.33	0.40	−0.18	0.41
200	0.50	0.08	0.27	0.40	−0.31	0.34
400	0.50	−0.04	0.13	0.40	−0.60	0.18
800	0.50	0.02	0.04	0.40	0.12	0.07
Case '100%'						
60	0.50	0.28	0.53	0.40	−0.24	1.02
100	0.50	0.32	0.53	0.40	−0.45	0.97
200	0.50	0.17	0.40	0.40	−0.61	0.70
400	0.50	0.04	0.27	0.40	−0.34	0.41
800	0.50	−0.02	0.07	0.40	−0.17	0.12

Table 4 Summary of simulation for CBF and OEF in the case '25%' and the case '100%' of ischemic model using the DARG method with the subtraction method

$CO–O_2$ time lag (s)	CBF			OEF		
	Average (mL/g/min)	Error (%)	COV (%)	Average	Error (%)	COV (%)
Case '25%'						
60	0.20	0.05	0.15	0.70	−0.13	0.46
100	0.20	0.05	0.14	0.70	−0.14	0.36
200	0.20	0.00	0.11	0.70	−0.25	0.29
400	0.20	−0.05	0.06	0.70	−0.51	0.16
800	0.20	0.01	0.02	0.70	0.11	0.06
Case '100%'						
60	0.20	0.09	0.25	0.70	−0.22	0.86
100	0.20	0.10	0.24	0.70	−0.36	0.83
200	0.20	0.03	0.17	0.70	−0.50	0.62
400	0.20	−0.01	0.11	0.70	−0.27	0.36
800	0.20	−0.02	0.04	0.70	−0.15	0.11

underestimation depended on the amount of $C^{15}O$ radioactivity, the time interval between the $C^{15}O$ scan and the $^{15}O_2$–$C^{15}O_2$ scan, and the disease model we assumed. By subtracting the $C^{15}O$ radioactivity from the input function and PET counts, this underestimation could be eliminated, which resulted in shortening the total study period of the DARG protocol.

Underestimation of CBF and OEF values due to residual $C^{15}O$ radioactivity

In general, overestimations of the arterial radioactivity or PET counts can cause underestimation or overestimation of physiological measures (CBF and OEF), respectively, in the DARG method. Thus, the residual $C^{15}O$ radioactivity might induce the bias in either of direction. As shown in our results, the estimated CBF and OEF values were both underestimated due to the residual $C^{15}O$ radioactivity, which indicates that the bias of the input function by the $C^{15}O$ radioactivity more strongly influenced the estimates than the bias of the PET counts by the $C^{15}O$ radioactivity. In our simulation, the CBV was fixed as 0.04 mL/mL. If the larger CBV was assumed (i.e. dilatation of blood vessel), more residual $C^{15}O$ radioactivity was added on the PET counts and the bias of the total PET counts was increased by Eq. 1, which results in less underestimation for the CBF and OEF values. Note that in this paper, we evaluated not $CMRO_2$ but OEF. $CMRO_2$ is derived by being multiplied CBF and OEF values. Thus, the magnitude of the underestimation in $CMRO_2$ could be larger than those of CBF and OEF.

Tables 1 and 2 suggest that the normal model underestimated OEF more than the ischemic model because of the residual $C^{15}O$ radioactivity. On other hand, the normal

model underestimated CBF less than the ischemic model because of the residual $C^{15}O$ radioactivity. Although the DARG method uses $^{15}O_2$ phase (PET data before the inhalation of $C^{15}O_2$) and $C^{15}O_2$ phase (PET data after the inhalation of $C^{15}O_2$) datasets, and simultaneously estimates CBF and OEF values, the PET data of the $^{15}O_2$ phase were dominant in the determination of OEF and those of the $C^{15}O_2$ phase were dominant in the determination of CBF. As shown in Tables 1 and 2, the amount of the underestimation for OEF is larger than for CBF, which can be explained by the amount of residual $C^{15}O$ radioactivity in both phases. As shown in Fig. 2, the influence of $C^{15}O$ on the input function was much higher in the $^{15}O_2$ phase than in the $C^{15}O_2$ phase. The residual $C^{15}O$ radioactivity led to the underestimation of CBF, mainly determined in the $C^{15}O_2$ phase. However, this underestimation was not enough to explain the bias of the input function in the $^{15}O_2$ phase. The first term on the right side of Eq. 1 has only CBF (f) as a parameter and the value of the first term is much higher in the normal model than in the ischemic model due to the higher CBF of the normal model, which implies that a greater underestimation for OEF could occur in the normal model to compensate for the insufficient underestimation of CBF. The ischemic model has a lower CBF than the normal model, which results in the slow washout of $^{15}O_2$ in tissue (the second term on the right side of Eq. 1). Therefore, the ischemic model has a greater source of underestimation for CBF than the normal model during the $C^{15}O_2$ phase.

As shown in Tables 1, 2, 3, and 4, the COVs of CBF and OEF in the ischemic model were smaller than the COVs in the normal model. The non-linear relationship between the PET counts and CBF attributed to this phenomenon [13]. The PET counts of the normal model were higher than those of the ischemic model, and the higher PET counts emphasized the noise due to this non-linearity.

Our results suggest that attention must be paid to the interpretation of CBF and OEF images from DARG, if contaminated by the significant amount of the residual $C^{15}O$ radioactivity namely: the magnitude of the error may not be uniform across different physiological conditions in the brain.

Subtraction method

The subtraction method successfully eliminated the influence of the $C^{15}O$ radioactivity on both the input function and PET counts during the $^{15}O_2$–$C^{15}O_2$ scan, and no errors in the CBF and OEF values due to the residual $C^{15}O$ radioactivity were observed. In theory, there is no statistical advantage for the subtraction method compared to the conventional method. However, as shown in Tables 3 and 4, the COV by the subtraction method was smaller than the value by the conventional method. It is necessary to separate the $^{15}O_2$ contents and $C^{15}O_2$ contents in the measured input function prior to the DARG calculation. For this separation, we utilized the linear method proposed by Kudomi et al. [16]. The linear method estimates the $^{15}O_2$ contents in the input function after $C^{15}O_2$ inhalation by linear extrapolation. In the conventional method, due to the offset of the input function by the residual $C^{15}O$ radioactivity, the estimated $^{15}O_2$ contents remain until the last in most cases. On other hand, in the subtraction method, by subtracting the $C^{15}O$ radioactivity from the input function, the offset of the input function is removed. Then, in many cases the $^{15}O_2$ contents estimated by the extrapolated line go to zero. This causes a reduction of the variation in the estimated CBF and OEF values compared to the conventional method.

The estimation of the recirculation water in the input function is based on the empirical model [10], and this model may not work owing to the residual $C^{15}O$ radioactivity, which results in biased CBF and OEF values. This bias can be removed by the subtraction method. Thus, by using the subtraction method, accurate CBF and OEF values can be measured no matter how much $C^{15}O$ radioactivity exists, which results in shortening the total PET study. The subtraction method could be applied, not only to the DARG protocol, but also to the conventional ARG and steady-state protocols. In this simulation, we assumed no biological decay of $C^{15}O$, which is not true in the actual data, and the subtraction method might over-subtract the influence of $C^{15}O$ radioactivity. The biological half-life of $C^{15}O$ is difficult to determine within a period of ordinary PET scan owing to the short life of the ^{15}O radionuclide. We tested simulated data with a biological half-life of 10 min, and there were no significant differences in the estimated CBF and OEF values compared to the results shown in this paper. In order to apply the subtraction method in clinical study, further studies are, however, required to verify the influence of biological decay.

Sequence of PET scans

In this paper, the sequence of the scans was a $C^{15}O$ scan followed by a $^{15}O_2$–$C^{15}O_2$ scan. If the $C^{15}O$ scan was performed after the $^{15}O_2$–$C^{15}O_2$ scan, our results were not valid. The reason for this sequence ($C^{15}O$ scan followed by a $^{15}O_2$–$C^{15}O_2$ scan) was to shorten the total duration of the PET study by exchanging the target gas (from N_2 containing O_2 to N_2 containing CO_2) only once (the synthesis of $C^{15}O$ and $^{15}O_2$ shares the same target in a cyclotron but uses different one from that of $C^{15}O_2$). Furthermore, the sequence of $^{15}O_2$–$C^{15}O_2$ produces better results than the sequence of $C^{15}O_2$–$^{15}O_2$ [15]. In order to further shorten the total study time, more development efforts are needed

in relation to the delivery system for the radioactive gases, which should have the ability to deliver such gases quickly.

The results in this paper were based only on the computer simulations. It could be expected to have several difficulties to show validities of our results using actual PET measurements by several reasons such as (1) PET cannot differentiate between photon from residual $C^{15}O$ and photon from either $^{15}O_2$ or $C^{15}O_2$, (2) large inter-subject variation for cerebrovascular disease, (3) large amounts of radiation exposure to patients from $C^{15}O$ in the case of large inhalation of $C^{15}O$. For the validation of our results, PET studies with ischemic animal model will be anticipated.

Conclusions

In this paper, we verified the influence of $C^{15}O$ radioactivity on the computation of CBF and OEF using the DARG protocol. We found that the bias and noise in the CBF and OEF values depended on the amount of residual $C^{15}O$ radioactivity during the scanning for $^{15}O_2$ and $C^{15}O_2$, and on the physiological conditions of the brain tissue. By using the subtraction method, the bias could be eliminated. Finally, we discussed the effects of the recirculation water and the biological decay for $C^{15}O$ radioactivity on the computation of CBF and OEF using the DARG method.

References

1. Frackowiak RS, Jones T, Lenzi GL, Heather JD. Regional cerebral oxygen utilization and blood flow in normal man using oxygen-15 and positron emission tomography. Acta Neurol Scand. 1980;62:336–44.
2. Frackowiak RS, Lenzi GL, Jones T, Heather JD. Quantitative measurement of regional cerebral blood flow and oxygen metabolism in man using 15O and positron emission tomography: theory, procedure, and normal values. J Comput Assist Tomogr. 1980;4:727–36.
3. Mintun MA, Raichle ME, Martin WR, Herscovitch P. Brain oxygen utilization measured with O-15 radiotracers and positron emission tomography. J Nucl Med. 1984;25(2):177–87.
4. Lammertsma AA, Jones T. Correction for the presence of intravascular oxygen-15 in the steady-state technique for measuring regional oxygen extraction ratio in the brain: 1. Description of the method. J Cereb Blood Flow Metab. 1983;3:416–24.
5. Subramanyam R, Alpert NM, Hoop B Jr, Brownell GL, Yaveras JM. A model for regional cerebral oxygen distribution during continuous inhalation of 15O2, C15O, and C15O2. J Nucl Med. 1978;19:48–53.
6. Lammertsma AA, Heather JD, Jones T, Frackowiak RS, Lenzi GL. A statistical study of the steady state technique for measuring regional cerebral blood flow and oxygen utilization using 15O. J Comput Assist Tomog. 1982;6:566–73.
7. Correia JA, Alpert NM, Buxton RB, Ackerman RH. Analysis of some errors in the measurement of oxygen extraction and oxygen consumption by the equilibrium inhalation method. J Cereb Blood Metab. 1985;5:591–9.
8. Okazawa H, Ymauchi H, Sugimoto K, Takahashi M, Toyoda H, Kishibe Y, et al. Quantitative comparison of the bolus and steady-state methods for measurement of cerebral perfusion and oxygen metabolism: positron emission tomography study using 15O-gas and water. J Cereb Blood Metab. 2001;21:793–803.
9. Okazawa H, Ymauchi H, Sugimoto K, Toyoda H, Kishibe Y, Takahashi M. Effects of acetazolamide on cerebral blood flow, blood volume, and oxygen metabolism: a positron emission tomography study with healthy volunteers. J Cereb Blood Flow Metab. 2001;21:1472–9.
10. Iida H, Jones T, Miura S. Modeling approach to eliminate the need to separate arterial plasma in oxygen-15 inhalation positron emission tomography. J Nucl Med. 1993;34:1333–40.
11. Sadato N, Yonekura Y, Senda M, Iwasaki Y, Matoba N, Tamaki N, et al. PET and the autoradiographic method with continuous inhalation of oxygen-15-gas: theoretical analysis and comparison with conventional steady-state methods. J Nucl Med. 1993; 34:1672–80.
12. Hatazawa J, Fujita H, Kanno I, Satoh T, Iida H, Miura S, et al. Regional cerebral blood flow, blood volume, oxygen extraction fraction, and oxygen utilization rate in normal volunteers measured by the autoradiographic technique and the single breath inhalation method. Ann Nucl Med. 1995;9:15–21.
13. Shidahara M, Watabe H, Kim KM, Oka H, Sago M, Hayashi T, et al. Evaluation of a commercial PET tomograph-based system for the quantitative assessment of rCBF, rOEF and rCMRO2 by using sequential administration of ^{15}O-labeled compounds. Ann Nucl Med. 2002;16(5):317–27.
14. Hattori N, Bergsneider M, Wu HM, Glenn TC, Vespa PM, Hovda DA, et al. Accuracy of a method using short inhalation of 15O–O2 for measuring cerebral oxygen extraction fraction with PET in healthy humans. J Nucl Med. 2004;45:765–70.
15. Kudomi N, Hayashi T, Teramoto N, Watabe H, Kawachi N, Ohta Y, et al. Rapid quantitative measurement of $CMRO_2$ and CBF by dual administration ^{15}O-labeled oxygen and water during a single PET scan—a validation study and error analysis in anesthetized monkeys. J Cereb Blood Flow Metab. 2005;25:1209–24.
16. Kudomi N, Watabe H, Hayashi T, Iida H. Separation of input function for rapid measurement of quantitative $CMRO_2$ and CBF in a single PET scan with a dual tracer administration method. Phys Med Biol. 2007;52(7):1893–908.
17. Kudomi N, Choi E, Yamamoto S, Watabe H, Kim KM, Shidahara M, et al. Development of a GSO Detector Assembly for a Continuous Blood Sampling System. IEEE Trans Nucl Sci. 2003; 50(1):70–3.
18. Carson RE. Parameter estimation in positron emission tomography. In: Phelps ME, Mazziotta JC, Schelbert HR, editors. Positron emission tomography and autoradiography. New York: Raven Press; 1986. p. 347–90.
19. Shidahra M, Watabe H, Kim KM, Kudomi N, Ito H, Iida H. Optimal scan time of oxygen-15-labeled gas inhalation autoradiographic method for measurement of cerebral oxygen extraction fraction and cerebral oxygen metabolic rate. Ann Nucl Med. 2008;22(8):667–75.
20. Ito H, Kanno I, Fukuda H. Human cerebral circulation: positron emission tomography studies. Ann Nucl Med. 2005;19(2):65–74.

利用技術

小動物の高解像度 SPECT イメージング

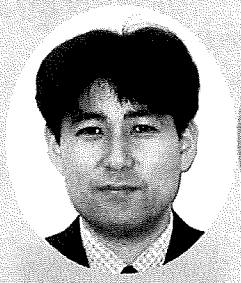
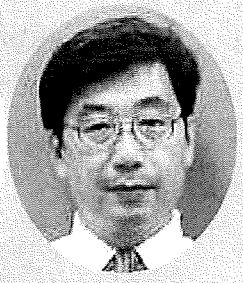

銭谷　勉　*Zeniya Tsutomu*
飯田　秀博　*Iida Hidehiro*
（国立循環器病センター研究所 先進医工学センター 放射線医学部）

1　はじめに

創薬や新規治療法の評価を目的とした前臨床研究において，マウスやラットを用いた小動物の *in vivo* イメージングは，同一の動物を非侵襲的に繰り返し検査できる点から，その要求は高い。特に，PET（Positron Emission Tomography）や SPECT（Single Photon Emission Computed Tomography）といった核医学検査装置は，高い感度でトレーサの挙動を観測できるため，病態生理や病態生化学的な変化を定量的に評価できる。遺伝子改変したマウスなどのイメージングにおいて，その利用価値が高いと考えられる。

実際に小動物を撮像する場合，サイズがヒトよりも相当小さいため，高い空間解像度が要求される。SPECT 装置の場合，ピンホールコリメータの拡大効果を利用することで比較的容易に高い解像度が得られる。現在，実用化されているほとんどの小動物用 SPECT 装置はピンホールコリメータを採用している。

本稿では，小動物の高解像度 SPECT イメージング技術及び我々の開発した小動物用 SPECT 装置を紹介し，最後にピンホール SPECT のヒトへの応用について述べる。

2　ピンホールコリメータを利用した高解像度 SPECT

SPECT 装置は原理的に放射性同位元素から放出される γ 線の飛来方向を特定するためのコリメータを必要とする。臨床用の SPECT 装置では，一般的にパラレルホールコリメータが用いられており，解像度は 10 mm 程度である。小動物イメージングでは対象臓器も小さいため，それに伴って，高解像度が要求される。図 1 のようにピンホールコリメータは撮像対象がコリメータに近いほど，小視野領域の像をより拡大できるため，空間解像度及び感度を高くで

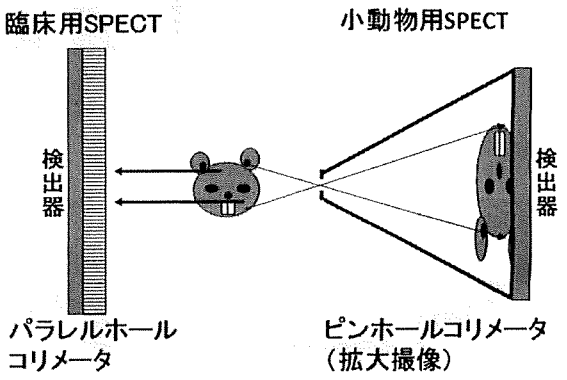

図 1　ピンホールコリメータによる拡大撮像

きる。1 mm 以下の解像度も比較的容易に実現できるため，小動物のイメージングに適している。

ピンホールコリメータを利用する技術は古くからあったが，研究の域を脱しなかった。それは，ピンホール SPECT で得られる画像は体軸方向に歪み，視野内で解像度が不均一になるため，定量評価が困難であったからである。我々はこの原因をデータの不完全に由来するものと仮説をたて，完全データを収集する撮像軌道を構築し，この軌道に対応する統計学に基づいた3次元画像再構成法を開発した。これによって，歪みのない視野全体で均一な解像度を有する3次元画像を得ることが可能になった（図 2）[1]。画像歪を改善する手法としては，他に，ヘリカル軌道による完全データ収集法，多数のピンホールを配列した近似的な完全データを収集する手法が開発されている。ただし，従来の撮像軌道でも統計学的3次元画像再構成を利用すれば視野の中央付近であれば歪みはある程度改善される。

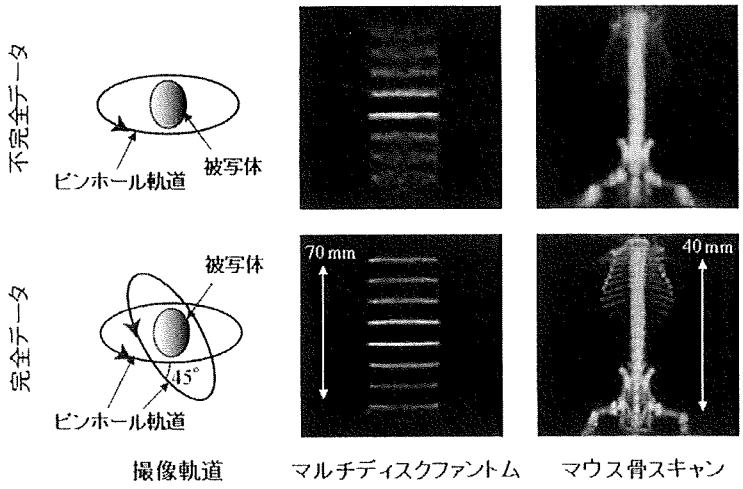

図 2　従来の単一円軌道による不完全データ（上）と2軸収集軌道による完全データ（下）から得られた再構成画像

3　小動物用 SPECT 装置

我々は，小型で可搬性のある小動物専用 SPECT 装置を開発した。装置を小型化するために導入した小型高解像度検出器は，大きさ 5 cm 程度であり，シンチレータが臨床用の平板 NaI に代えて，1.5 mm ピッチのピクセル型 NaI で，光電子増倍管（Photomultiplier Tube：PMT）も従来の2あるいは3インチの大型 PMT に代えて，6 mm の PMT で構成されている。小型高解像度検出器とピンホールコリメータの拡大撮像技術を組み合わせて[2]，コンパクトな小動物専用高解像度 SPECT 装置を開発した（図 3(a)）。本装置では，ピンホールコリメータの弱点でもある低感度を補うため，被写体の周囲に4台の検出器が 90° 間隔で配列されている。また，小動物ベッドが水平方向に回転可能となっており，異なる回転軸による撮像軌道で完全データ収集が可能である。

マルチラインソースファントム実験では，1.3 mm 径のラインが識別可能であった（図 3(b)）。また，本装置を用いて，覚醒下で，健常ラットの心筋血流量及び血管反応性が評価可能であることを実証した。図 3(c) は本実験で

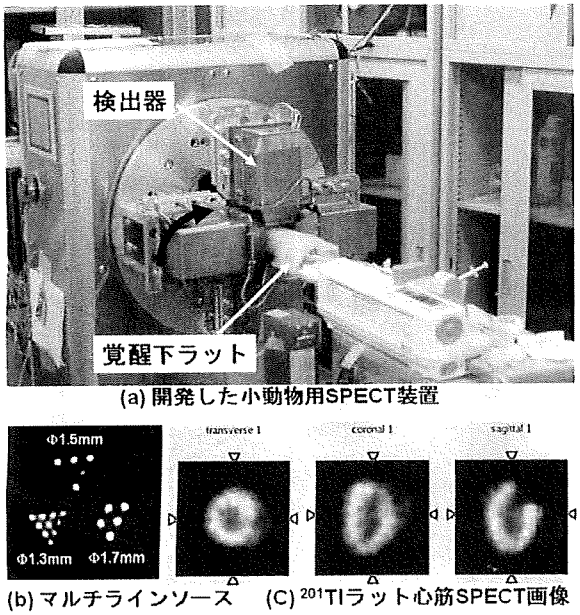

図 3　小動物用 SPECT 装置と再構成画像

得られたラット心筋SPECT画像であるが，非常に鮮明である。

4 ピンホールSPECTによるヒト局所高解像度撮像

従来，ピンホールSPECTのような小視野でヒトのような大きな被写体を撮像した場合，データ欠損(トランケーション)が生じ，それによるアーチファクトや過大評価のため，定量評価は困難であった。そこで，我々はピンホールSPECTにおいてトランケーションを許す画像再構成法を開発した[3]。図4のように視野内に被写体の外側のゼロカウント領域（既知領域）を含むこと，画像再構成領域が被写体全体を含むこと，この2つの条件下で逐次近似による画像再構成を行うことによって，視野内はトランケーションの影響なく，正しい画像が得られる。このことを脳ファントム実験によって実証した（図4）。臨床SPECTでは低解像度で詳細構造は見えなかった。また，ピンホールSPECTデータを従来法で再構成した場合はアーチファクトが見られ，視野全域でカウントが過大評価されていた。一方，ピンホールSPECTデータを開発した手法で画像再構成した場合，アーチファクトも過大評価もなく，高解像度で詳細構造が描出された。

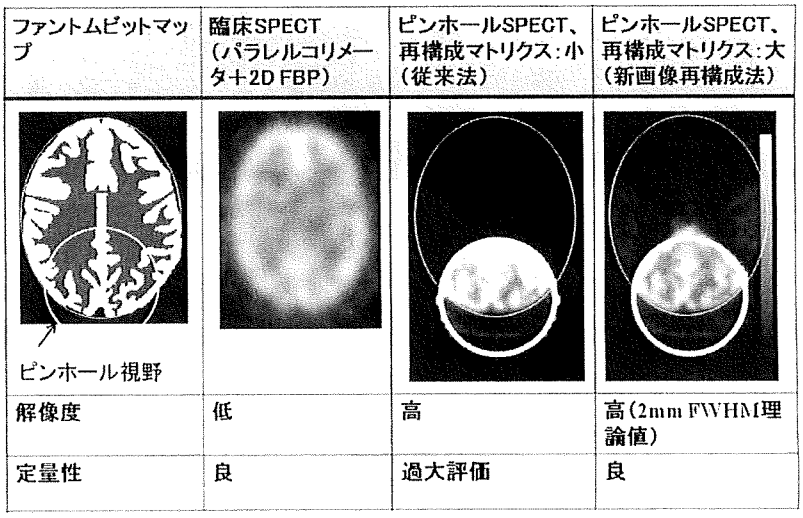

図4 脳ファントムの再構成画像
ピンホールSPECTと新再構成法によって，アーチファクトや過大評価がなく，詳細構造が明瞭に描出された

本撮像技術によって，微小腫瘍検出，血管プラークイメージング，てんかん焦点同定，部分容積効果のない血流定量などが可能になると考えられる。

5 おわりに

現在，小動物の高解像度SPECTイメージングはピンホールコリメータと撮像法の工夫によって実用化の域に達した。さらに，小動物撮像で培われた高解像度技術はヒトの撮像へ応用されようとしている。

参考文献

1) Zeniya T, *et al.*：*Eur J Nucl Med Mol Imaging*, **31**, 1166-1172 (2004)
2) Zeniya T, *et al.*：*Ann Nucl Med*, **20**, 409-416 (2006)
3) Zeniya T, *et al.*：*IEEE 2007 Nuclear Science Symposium Conference Record*, **6**, 4205-4207 (2007)

Journal of Cerebral Blood Flow & Metabolism (2008), 1–10

www.jcbfm.com

A physiologic model for recirculation water correction in $CMRO_2$ assessment with $^{15}O_2$ inhalation PET

Nobuyuki Kudomi, Takuya Hayashi, Hiroshi Watabe, Noboru Teramoto, Rishu Piao, Takayuki Ose, Kazuhiro Koshino, Youichirou Ohta and Hidehiro Iida

Department of Investigative Radiology, Advanced Medical-Engineering Center, National Cardiovascular Center Research Institute, Osaka, Japan

Cerebral metabolic rate of oxygen ($CMRO_2$) can be assessed quantitatively using $^{15}O_2$ and positron emission tomography. Determining the arterial input function is considered critical with regards to the separation of the metabolic product of $^{15}O_2$ (RW) from a measured whole blood. A mathematical formula based on physiologic model has been proposed to predict RW. This study was intended to verify the adequacy of that model and a simplified procedure applying that model for wide range of species and physiologic conditions. The formula consists of four parameters, including of a production rate of RW (*k*) corresponding to the total body oxidative metabolism ($BMRO_2$). Experiments were performed on 6 monkeys, 3 pigs, 12 rats, and 231 clinical patients, among which the monkeys were studied at varied physiologic conditions. The formula reproduced the observed RW. Greater *k* values were observed in smaller animals, whereas other parameters did not differ amongst species. The simulation showed $CMRO_2$ sensitive only to *k*, but not to others, suggesting that validity of determination of only *k* from a single blood sample. Also, *k* was correlated with $BMRO_2$, suggesting that *k* can be determined from $BMRO_2$. The present model and simplified procedure can be used to assess $CMRO_2$ for a wide range of conditions and species.
Journal of Cerebral Blood Flow & Metabolism advance online publication, 5 November 2008; doi:10.1038/jcbfm.2008.132

Keywords: arterial input; $CMRO_2$; mathematical modeling; recirculation water; PET

Introduction

Cerebral metabolic rate of oxygen ($CMRO_2$) can be quantitatively assessed using ^{15}O-labeled oxygen ($^{15}O_2$) and positron emission tomography (PET). This technique is based on an estimation of influx rate of $^{15}O_2$ to the cerebral tissue from arterial blood. Using information of cerebral blood flow (CBF) that may be obtained either from a separate scan with ^{15}O-labeled water ($H_2^{15}O$) or from the clearance rate $^{15}O_2$ of tissue, the oxygen extraction fraction (OEF) can also be calculated. The arterial input function must be determined before beginning this calculation. More specifically, a metabolic product of $^{15}O_2$ in the arterial blood, as a form of ^{15}O-labeled water (i.e., recirculating ^{15}O-water or RW) needs to be accurately estimated.

The arterial whole blood radioactivity curve can be obtained by measuring the radioactivity concentration of continuously withdrawn whole blood using a monitoring device (Eriksson *et al*, 1988; Eriksson and Kanno, 1991; Votaw and Shulman, 1998; Kudomi *et al*, 2003). Assessment of a time-dependent RW curve may be achieved by separating the plasma from the whole blood samples. This, however, requires labor-intensive procedures of frequent, manual arterial blood samplings, the centrifugation of all collected blood samples, and radioactivity measurements for both whole blood and plasma (Holden *et al*, 1988).

Ohta *et al* (1992) proposed to neglect the component of RW from the arterial input function. This technique fits three parameters of $CMRO_2$, CBF, and

Correspondence: Dr H Iida, Department of Investigative Radiology, Advanced Medical-Engineering Center, National Cardiovascular Center Research Institute, 5-7-1, Fujishirodai, Suita, Osaka 565-8565, Japan.
E-mail: iida@ri.ncvc.go.jp
This study was supported by the Program for Promotion of Fundamental Studies in Health Science of the Organization for Pharmaceutical Safety and Research of Japan, a Grant for Research on Advanced Medical Technology from the Ministry of Health, Labour and Welfare (MHLW), Japan, and by Nakatani Electronic Measuring Technology Association of Japan (NK).
Received 2 May 2005; revised 6 October 2008; accepted 11 October 2008

cerebral blood volume (CBV) to the kinetic $^{15}O_2$ data obtained from a single PET scan after the bolus administration of $^{15}O_2$. To minimize errors which result from neglecting RW, only the initial 3 mins of data after the bolus inhalation of $^{15}O_2$ were used when calculating the parameters. This approach has been applied to evaluate the magnitude of increase in $CMRO_2$ relative to that in CBF during cognitive stimulation tasks (Fujita *et al*, 1999; Vafaee and Gjedde, 2000; Okazawa *et al*, 2001*a*, *b*; Yamauchi *et al*, 2003; Mintun *et al*, 2002), but one of the drawbacks to this technique is the lack of accurate statistics, which is due to the use of a short scan duration.

Iida *et al* (1993) have developed a mathematical formula to predict the production of RW based on a physiologic model, which allows prolongation of the PET acquisition period with an additional statistical accuracy. The formula assumes a fixed rate constant for production of RW from $^{15}O_2$ in the body. This is based on the fact that the observed rate constant did not vary among clinical subjects, and thus causes nonsignificant errors in $CMRO_2$. However, the study is limited only to human subjects studied at rest, and results have not been verified using other species such as rat and mouse (Magata *et al*, 2003; Temma *et al*, 2006; Yee *et al*, 2006). Also, the findings have not been evaluated on humans who are under physiologic stress, though under such conditions the whole-body oxygen consumption is expected to change. Moreover, it is important to extend the approach to physiologically stressed conditions as recent progress for assessing $CMRO_2$ and CBF simultaneously from a short period dynamic scan by using a dual tracer autoradiography (DARG) (Kudomi *et al*, 2005). The DARG has enabled the $^{15}O_2$ PET to assess $CMRO_2$ and CBF simultaneously at various physiologically activated conditions.

The aim of this study is to verify the method used to estimate the arterial RW during the $^{15}O_2$ inhalation for simultaneous determination of $CMRO_2$ and CBF from the rapid procedures of $^{15}O_2$ PET. The feasibility of a simplified procedure is also being investigated. Applicability of this approach was tested for a wide range of species under various physiologic conditions. Experiments were designed to apply for different species as well as different physiologic conditions. A simulation study was also performed to evaluate the level of error sensitivity associated with this approach.

Materials and methods

Theory

Variables used in the recirculating water model are summarized in Table 1. The mathematical model that formulates the time-dependent RW in arterial blood consists of three rate constants: (1) the production rate of RW or k (per min), proportional to oxidative metabolism in the total body system ($BMRO_2$), (2) the forward diffusion rate (k_w, per min) of the metabolized ^{15}O-water between the blood and interstitial spaces in the body, and (3) the backward diffusion rate (k_2, per min) of the metabolized ^{15}O-water between the blood and interstitial spaces in the body. The differential equations for the arterial activity concentration of ^{15}O-water at a time t (secs) ($A_w(t)$, Bq/mL), after the physical decay correction can be expressed as follows (Huang *et al*, 1991):

$$\frac{d}{dt}A_w(t) = k \cdot A_o(t) - k_w \cdot A_w(t) + k_2 \cdot C(t) \quad (1a)$$

$$\frac{d}{dt}C(t) = k_w \cdot A_w(t) - k_2 \cdot C(t) \quad (1b)$$

$$A_t(t) = A_o(t) + A_w(t) \quad (1c)$$

where $A_o(t)$ and $A_t(t)$ denote the radioactivity concentration of the arterial $^{15}O_2$ and the total radioactivity from both

Table 1 Variables used in the recirculating water model

Symbol	*Description*	*Unit*
A_o	Radioactivity concentration of arterial $^{15}O_2$	Bq/mL
A_w	Radioactivity concentration of arterial $H_2^{15}O$	Bq/mL
A_t	Total radioactivity concentration from arterial $^{15}O_2$ and $H_2^{15}O$	Bq/mL
A_{plasma}	Radioactivity concentration of arterial plasma	Bq/mL
C	Activity concentration of $H_2^{15}O$ in peripheral tissue in a body	Bq/mL
Fi_{O_2}	Oxygen concentration in inhaled gas	%
Fe_{O_2}	Oxygen concentration in expired gas	%
k	Production rate of recirculating $H_2^{15}O$	per min
k_{BM}	Production rate of recirculating $H_2^{15}O$ obtained from BM approach	per min
k_w	Forward diffusion rate of $H_2^{15}O$ from blood to body interstitial space	per min
k_2	Backward diffusion rate of $H_2^{15}O$ from blood to body interstitial space	per min
λ	Decay constant of ^{15}O (=0.00567 per sec)	per sec
v	Stroke volume	mL
p	k_w/k_2	
r	Respiration rate	per min
R	Fractional water content ratio in whole blood to that in the plasma	
R_{O_2}	Rate of oxidative metabolism in the whole-body system	mL/min
Δt	Delayed appearance time of recirculating water	secs
V_{O_2}	Total volume of molecular oxygen in total blood	mL
V_{TB}	Total volume of blood in a body	mL

$^{15}O_2$ and $H_2^{15}O$, respectively. $C(t)$ is an activity concentration of $H_2^{15}O$ in the peripheral tissue of the total body. Assuming a delayed appearance of RW by Δt (Iida *et al*, 1993), the following equation can be obtained:

$$A_w(t+\Delta t) = k(\alpha_1 \cdot A_t(t) \otimes \exp(-\beta_1 t) + \alpha_2 \cdot A_t(t) \otimes \exp(-\beta_2 t)) \quad (2)$$

where $\otimes$ denotes the convolution integral and:

$$\alpha_{1,2} = \frac{a - 2c \pm \sqrt{a^2 - 4b}}{\pm 2\sqrt{a^2 - 4b}}, \qquad \beta_{1,2} = \frac{a \pm \sqrt{a^2 - 4b}}{2},$$
$$a = k + k_w + k_w/p, \quad b = k \cdot k_w/p, \quad c = k_w/p, \quad p = k_w/k_2 \quad (3)$$

Following four approaches were performed to determine the rate constants and $A_w(t)$.

Approach by four parameters fitting: Four parameters, k, Δt, k_w, and p $(=k_w/k_2)$, can be determined from the observed RW ($A_w(t)$) and the $A_t(t)$ curves by means of the nonlinear least square fitting (4PF approach).

Approach by one parameter fitting: Once three parameters, Δt, k_w, and p, are fixed by averaging values determined by the 4PF approach, k can then be determined by fitting the Equation 2 to measured $A_w(t)$ from $A_t(t)$ (1PF approach). In this procedure, single datum is sufficient, and thus k can be determined from $A_t(t)$ and the RW counts sampled at a single time point.

Approach from steady-state condition: Similarly to the 1PF procedures, k can be determined from the steady state condition, which is achieved by a continuous administration of $^{15}O_2$ as follows (SS approach). Incorporating the decay constant of ^{15}O ($\lambda = 0.00567$ per secs) into Equations 1a and 1b provides:

$$\frac{d}{dt}A^*_w(t) = k \cdot A^*_o(t) - k_w \cdot A^*_w(t) + k_2 \cdot C^*(t) - \lambda \cdot A^*_w(t) \quad (4a)$$

$$\frac{d}{dt}C^*(t) = k_w \cdot A^*_w(t) - k_2 \cdot C^*(t) - \lambda \cdot C^*(t) \quad (4b)$$

where variables with the symbol * denote that no correction was made for the radioactivity decay of ^{15}O. After continuously administrating $^{15}O_2$, the radioactivity distribution of $A^*_o(t)$, $A^*_w(t)$, and $C^*_t(t)$ reaches a steady state. Thus, the following equations hold:

$$0 = k \cdot A^*_o(t) - k_w A^*_w(t) + k_2 C^*(t) - \lambda A^*_w(t) \quad (5a)$$

$$0 = k_w A^*_w(t) - k_2 C^*(t) - \lambda C^*(t) \quad (5b)$$

Given the values of k_w and k_2 which are determined as averages of 4PF, k can be calculated from the arterial $^{15}O_2$ and $H_2^{15}O$ concentrations at steady state as follows:

$$k = \lambda\left(\frac{k_w + k_2 + \lambda}{k_2 + \lambda}\right)\frac{A^*_w(t)}{A^*_o(t)} \quad (6)$$

Approach by the rate of whole body oxidative metabolism: In this study, an alternative approach is provided to obtain k, from the rate of oxidative metabolism in the whole-body system (BM approach). With this alternative approach, we assume that the production rate of RW or k is proportional to the rate of oxidative metabolism in the whole-body system (i.e., $BMRO_2$ (R_{O_2}, mL/min)). The rate of oxidative metabolism may change dependent on physiologic status of the subject. In addition, we assumed that this index can be defined from the difference of oxygen concentration between inhaled and exhaled trachea air samples. Therefore, the above can be expressed as follows:

$$k = c \cdot \frac{R_{O_2}}{V_{O_2}} \ (\text{per min}) \quad (7a)$$

or

$$k_{BM} = \frac{k}{c} = \frac{R_{O_2}}{1.36 \cdot Hb \cdot V_{TB}} \quad (7b)$$

where c is the proportionality constant, k_{BM} the production rate of RW obtained from BM approach, V_{O_2} (mL) the total volume of molecular oxygen in total blood, 1.36 mL/g the amount of oxygen molecules combined with unit mass of hemoglobin, Hb (g/mL) represents the hemoglobin concentration in the arterial blood, and V_{TB} (mL) is the total volume of blood in the body.

Simulation

A series of simulation studies were performed to investigate the effects of errors on estimated $CMRO_2$ value in the model parameters (k, Δt, k_w, and p). In these simulations, a typical arterial blood time activity curve (TAC) of $^{15}O_2$ and $H_2^{15}O$ after DARG protocol (Kudomi *et al*, 2005) obtained in a monkey study was used. RW TACs were generated from the whole blood TAC by assuming baseline values of k as 0.13, 0.11, 0.34, and 0.73 per min, Δt as 20, 11, 5, and 3 secs, k_w as 0.38, 0.43, 0.98, and 0.87 per min, and p as 1.31, 1.01, 0.98, and 0.83, corresponding to humans, pigs, monkeys, and rats, respectively. Tissue TACs were generated by assuming CBF = 50 mL/min per 100 g and OEF = 0.4 ($CMRO_2$ was defined as: $CMRO_2 = CBF \times OEF \times C_aO_2$, where C_aO_2 is the arterial oxygen content. This simulation was intended to investigate magnitude of error as a percentage difference, so that arbitrary value of C_aO_2 was assumed) (Hayashi *et al*, 2003), using a kinetic formula for oxygen and water in the brain tissue (Mintun *et al*, 1984; Shidahara *et al*, 2002; Kudomi *et al*, 2005). $CMRO_2$ values were calculated by the DARG method (Kudomi *et al*, 2005), in which RW TACs were separated from the whole blood by changing k from 0.0 to 1.0 per min, Δt from 0 to 30 secs, k_w from 0.0 to 2.0 per min, and p from 0.0 to 2.0, respectively. Errors in the estimated $CMRO_2$ were presented as a percentage difference from the assumed true values.

Subjects

Subjects consisted of four groups including monkeys, pigs, rats, and clinical patients. Monkeys were six healthy *macaca fascicularis* with body weight of 5.2 ± 0.8 kg and age ranging from 3- to 4-year old. Pigs were three farm pigs

with body weight of 38 ± 9 kg and age from 4 to 12 months. Rats were 12 male Wistar rats with body weight of 300 ± 54 g and age from 7 to 8 weeks. All animals were studied during anesthesia. The animals were maintained and handled in accordance with guidelines for animal research on Human Care and Use of Laboratory Animals (Rockville, National Institute of Health/Office for Protection from Research Risks, 1996). The study protocol was approved by the Subcommittee for Laboratory Animal Welfare of National Cardiovascular Center.

Human data were retrospectively sampled from an existing database at National Cardiovascular Center which documented subjects who underwent PET examination after the ^{15}O-steady-state protocol. There were 231 total samples, with body weight and age ranging from 58 ± 10 kg, and 63 ± 14 years, respectively. Only the arterial $^{15}O_2$ and $H_2^{15}O$ radioactivity concentrations measured at the steady-state condition were used for the present analysis.

Experimental Protocol

The six monkeys were anesthetized using propofol (4 mg/kg/h) and vecuronium (0.05 mg/kg/h) assigned as a baseline in contrast to the after physiologically stimulated conditions. Animals were intubated and their respiration was controlled by an anesthetic ventilator (Cato, Drager, Germany). Each monkey inhaled 2,200 MBq $^{15}O_2$ for 20 secs. After 3 mins, the monkeys were injected with 370 MBq $H_2^{15}O$ for 30 secs by the anterior tibial vein. This was aimed at assessing both CBF and $CMRO_2$ according to the DARG technique (Kudomi *et al*, 2005). At 30 secs before inhaling $^{15}O_2$ to the monkeys, arterial blood was withdrawn from the femoral artery for 420 secs at a rate of 0.45 mL/min using a Harvard pump (Harvard Apparatus, Holliston, MA, USA). The whole blood TAC was measured with a continuous monitoring system (Kudomi *et al*, 2003) and the $A_t(t)$ was obtained. Meanwhile, we also manually obtained 0.5 mL of arterial blood samples from the contralateral femoral artery at 30, 50, 70, 90, 110, 130, 160, 190, and 360 secs after the $^{15}O_2$ inhalation. For the analysis of sampled blood, 0.2 mL of the blood were used for measurement of the radioactivity concentration of the whole blood, and the rest of the blood sampled (~0.3 mL) was immediately centrifuged for separation to measure the plasma radioactivity concentration ($A_{plasma}(t)$, Bq/mL). The radioactivity concentration was measured using a well counter (Molecular Imaging Laboratory Co. Ltd, Suita, Japan).

In two monkeys, anesthetic level was changed by altering the injection dose of propofol from 4 (baseline) to 8 and then to 12 and 16 mg/kg/h in one monkey, and to 5 and then to 7, 10, and 15 mg/kg/h in the other. In another monkey, $PaCO_2$ level was varied from 39 (baseline) to 47, and then to 33, 26, and 42 mm Hg by changing the respiratory rate. Each measurement for $^{15}O_2$ inhalation and $H_2^{15}O$ injection was initiated after at least 30 mins of applying the physiologic stimulation to achieve a steady state. All procedures were the same as those for the baseline, with the exception of the manual blood sample, which was obtained only once at 70 secs.

Before and after 6 mins of the $^{15}O_2$ inhalation, oxygen concentration in both inhaled (Fi_{O_2}, %) and end-tidal expiratory gas (Fe_{O_2}, %) was measured by the anesthetic ventilator in five out of the six monkeys. Using the respiration rate (r, per min) and the stroke volume (v, mL) indicated on the ventilator, the $BMRO_2$ (R_{O_2} mL/min) was calculated using the following equation:

$$R_{O_2} = (Fi_{O_2} - Fe_{O_2}) \cdot v \cdot r.$$

All monkeys received a PET measurement to assess the $CMRO_2$ at physiologically baseline condition. The scan protocol followed the DARG technique (Kudomi *et al*, 2005) in which a 6-mins single dynamic PET scan was performed in conjunction with the administration of dual tracers (i.e., $^{15}O_2$ followed by $H_2^{15}O$ after a 3-mins interval). PET scanner used was ECAT HR (Siemens-CTI, Knoxville, TN, USA), which provided 47 tomographic slice images for an axial field-of-view of approximately 150 mm. We performed arterial–sinus blood sampling to obtain a global OEF (OEF_{A-V}) (A–V difference approach). We sampled 0.2 mL of arterial and sinus blood simultaneously during each PET scan and measured their oxygen content (C_aO_2 and C_vO_2, respectively) (Kudomi *et al*, 2005). The OEF_{A-V} was calculated as: $OEF_{A-V} = (C_aO_2 - C_vO_2)/C_aO_2$.

With regards to the farm pigs involved in this experiment, we used existing data, which were originally obtained in one of the myocardial projects. During the study, three farm pigs were anesthetized. Anesthesia was induced by ketamine (10 mg/kg) and maintained using propofol (4 mg/kg/h). Animals were intubated and their respiration was controlled by the anesthetic ventilator. Venous blood was labeled with $^{15}O_2$ using a small artificial lung unit (Magata *et al*, 2003). $^{15}O_2$-labeled blood (222 to 700 MBq) was injected for 10 secs via anterior tibial vein. At 30 secs before this injection, arterial blood was withdrawn from the femoral artery at a rate of 0.45 mL/min using the Harvard pump and continued for 420 secs. The whole blood TAC ($A_t(t)$) was then measured with a continuous monitoring system (Kudomi *et al*, 2003). Meanwhile, we manually sampled 0.5 mL of arterial blood from the contralateral femoral artery at 30, 60, 90, 90, 120, 180, 240, and 300 secs after the $^{15}O_2$-labeled blood injection. For the analysis of sampled blood, 0.2 mL of the blood were used for measurement of the radioactivity concentration of the whole blood, and the rest of the blood sampled (~0.3 mL) was immediately centrifuged for separation to measure the plasma radioactivity ($A_{plasma}(t)$, Bq/mL). The radioactivity was measured using the well counter.

Data for rats were also originally obtained for other projects, and only the blood counts were used in this study. Anesthesia was induced with pentobarbital (50 mg/kg). A 10 mL of venous blood was labeled $^{15}O_2$ using a small artificial lung unit as described previously (Magata *et al*, 2003), and approximately 1 mL of $^{15}O_2$-labeled blood (37 to 74 MBq) was injected for 30 secs via the tail vein. Arterial blood samples of 0.1 mL each were obtained from the femoral artery at 5-secs intervals for 60 secs and 10-secs intervals for another 60 secs after the injection. Whole blood radioactivity concentration was measured using the well counter to be used as $A_t(t)$. Arterial blood samples of

0.2 mL each were obtained at 30, 60, 90, and 120 secs, and the plasma radioactivity concentration ($A_{plasma}(t)$) was measured by the well counter.

For clinical patients, the blood radioactivity concentration was obtained from previously performed PET examinations, which followed the steady-state protocol (Hirano *et al*, 1994). Each patient inhaled both $^{15}O_2$ and $C^{15}O_2$ to reach the steady state with an inhalation dose of approximately 1,200 and 500 MBq/min, respectively. Five to seven arterial blood samples were obtained during the steady state from the brachial artery. Mean values of radioactivity concentration of the whole blood and plasma, $A_t(t)$ and $A_{plasma}(t)$, respectively, were obtained for both $^{15}O_2$ and $C^{15}O_2$ PET examination.

Data Analysis

Using the blood activity data obtained from monkeys, pigs, and rats at baseline conditions, k as well as Δt, k_w and p were first determined by the 4PF approach, in which Equation 2 was applied to fit the $A_w(t)$ using the observed $A_t(t)$. Because the solubility of the oxygen is negligibly small in the plasma, we assumed that all radioactivity in plasma fraction comes from $H_2^{15}O$ and that the water content ratio of whole blood to plasma (R) does not change during measurement, which means that the kinetics of water molecules immediately reach equilibrium between the plasma and the cellular fraction (Mintun *et al*, 1984; Iida *et al*, 1993). Thus, $A_w(t)$ was obtained from the equation: $A_w(t) = A_{plasma}(t) \cdot R$, where R value was obtained from the sampled blood at the end of the scan (at which all the radioactivity in the blood can be considered as coming from $H_2^{15}O$ because inhaled $^{15}O_2$ is all metabolized).

Given that the values of Δt, k_w, and p were averages determined from 4PF for monkeys, pigs, and rats, only k was determined by fitting Equation 2 to A_w. This was calculated at various points in time, more specifically, in 30, 50, 70, 90, 110, 130, 160, and 190 secs for monkeys, in 30, 60, 90, 90, 120, 180, and 240 secs for pigs, and in 30, 60, 90, and 120 secs for rats. The optimal time point for k under the 1PF approach was determined, so that $(k_{4PF}-k_{1PF})/k_{4PF}$ reaches a minimal value. Here, k_{4PF} and k_{1PF} denote k values determined by the 4PF and 1PF approaches, respectively. The values of k in monkeys at baseline condition, together with those in pigs and rats were compared between 4PF and 1PF approaches, in which a k value from the optimal single time point was used.

In three of the monkeys, which were physiologically stimulated, k of 1PF approach was obtained using single time point of A_w. Assuming the total blood volume (V_{TB}) for monkeys as 360 mL (Lindstedt and Schaeffer, 2002), and using Hb as measured value in each experiment, k_{BM} was calculated from R_{O_2} according to Equation 7b. Then, k_{BM} obtained as: $k_{BM} = 0.00204R_{O_2}$ was compared with k determined by 1PF.

For clinical data obtained from the steady-state (SS approach) PET examinations, Equation 6 was used to determine the k values of the SS approach for each patient, in which values of k_w and k_2 were 0.38 and 0.29 per min as obtained in a previous work by Huang *et al* (1991).

$CMRO_2$ and OEF values in monkeys at baseline condition were calculated using the RW TACs obtained by four different methods (i.e., directly measured $A_w(t)$ ($n=6$), 4PF ($n=6$), 1PF ($n=6$), and BM approaches ($n=5$)). Regions-of-interest were selected for over the whole brain, and $CMRO_2$ and OEF values were obtained in those regions-of-interest. The $CMRO_2$ values compared among the four methods mentioned above to estimate RW TACs. The Bland–Altman method was applied to analyze the agreement of OEF values between the methods. Also, OEF values were compared with OEF_{A-V}.

All data were presented as mean ± 1 standard deviation. Student's t-test was used and Pearson's regression analysis was applied to compare two variables. A probability value of <0.05 was considered statistically significant.

Results

Figure 1 shows results from the simulation study, and shows the magnitude of errors in $CMRO_2$ calculated by the DARG method as well as errors in the parameters, k, Δt, k_w, and p. Errors in $CMRO_2$ were most sensitive to errors in k amongst all species, namely the production rate constant of RW in the arterial blood. After errors in k, errors in $CMRO_2$ were sensitive to errors in Δt. Errors in k_w and p, however, appeared to cause relatively insignificant errors in $CMRO_2$. More specifically, only 5 to 10% errors are caused in $CMRO_2$ by a change of ± 50% in k_w and p.

Figures 2A–2C show examples of the arterial whole blood curves (A_t) and RW TAC (A_w) observed in typical studies on a monkey, a pig, and a rat, respectively. The RW curves became constant after a period in all species. The rise time or appearance of the RW curves, $A_w(t)$, was significantly delayed compare to that of whole blood curve, $A_t(t)$. $A_w(t)$ curves fitted by 4PF well reproduced the measured RW curves in three species: monkeys, pigs, and rats. Table 2 summarizes values of k, Δt, k_w, and p obtained by the four parameter fitting (4PF approach), at the baseline for monkeys, pigs, and rats, and also k value obtained by the steady-state formula for clinical patients. Those comparisons showed that the k was significantly different among species ($P<0.001$) except between pig and human subjects, and it was significantly lower in smaller animals. Likewise, Δt showed significant differences among the three species ($P<0.001$), and it was also lower in smaller animals.

Table 3 summarizes k and $CMRO_2$ values obtained from a series of PET experiments performed on six monkeys at baseline condition, and for increased anesthesia (in two monkeys), and changed $PaCO_2$ levels (in one monkey). The best agreement of k values between 4PF and 1PF approaches was obtained from the blood sample data taken at 60, 70, and 60 secs in pigs, monkeys, and rats, respectively, and was used in the 1PF approach. With this

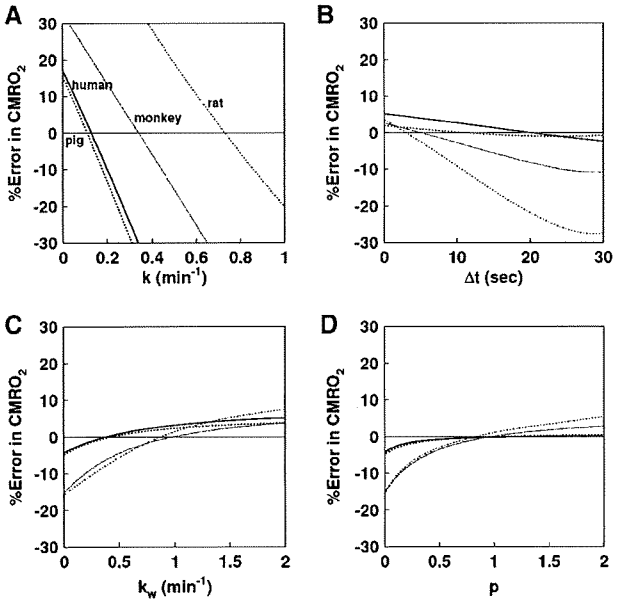

Figure 1 Error in $CMRO_2$ values due to errors in (**A**) k, (**B**) Δt, (**C**) k_w, and (**D**) p for assumed human, pig, monkey and rat. The same type of line indicates the same species. The percentage differences in the $CMRO_2$ values from the assumed true values (Table 1) were plotted as a function of the simulated value of k, Δt, k_w, and p.

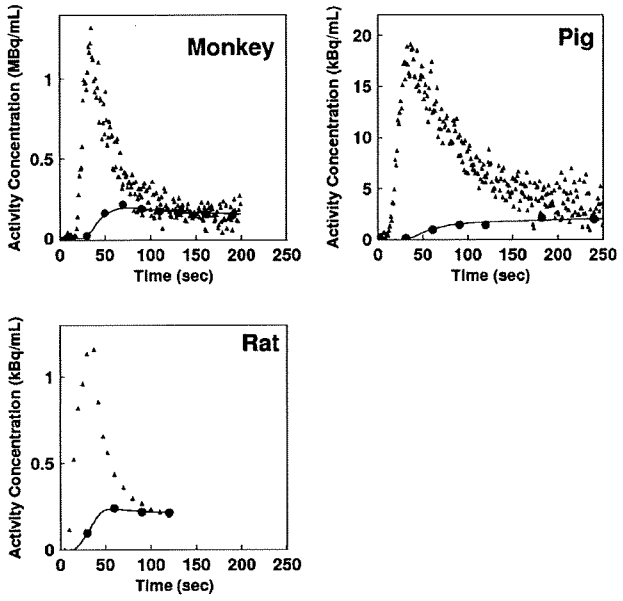

Figure 2 Representative comparison of the measured arterial whole blood and RW time activity curves for monkey, pig, and rat. Closed triangles and closed circles represent the measured whole blood and RW time activity curves, respectively. Estimated time activity curves by 4PF approach were also plotted in a solid line, and indicated a good agreement with the measured one.

optimized calibration protocol, k values were in a good agreement between 4PF and 1PF approaches. As shown in Figure 3, the regression analysis showed significant correlation for 21 animals including 6 monkeys, 3 pigs, and 12 rats ($P<0.001$), and there was no significant difference between the two variables. Figure 4 shows that k values calculated by the 1PF approach (at an optimized time) were in a good agreement with those calculated with the $BMRO_2$. Namely, the regression analysis showed significant correlation ($P<0.001$, $n=16$) and also that there was no significant difference between the two variables. Note that, in the $CMRO_2$ calculation by $BMRO_2$, k values were normalized according to the regression line shown in Figure 4. It should also be noted that calculated $CMRO_2$ values at the baseline shown in Table 3 were not significantly different among the four techniques. The average ($\pm$s.d.) values of obtained OEF were 0.53 ± 0.08, 0.52 ± 0.09, 0.54 ± 0.08, 0.54 ± 0.09, and 0.56 ± 0.04 from A–V difference, directly RW measured approach, 4PF, 1PF, and BM approaches, respectively. The Bland–Altman analysis of OEF values between from A–V difference and from others showed small over/underestimation, that is., with bias $\pm$ s.d. of -0.02 ± 0.09, 0.01 ± 0.07, 0.01 ± 0.08, and 0.02 ± 0.09, by direct RW, 4PF, 1PF, and BM approaches, respectively. Neither of the current methods (direct RW, 4PF, 1PF, and BM) was significantly different from A–V difference approach.

Discussion

Our study showed that the mathematical formula based on the physiologic model that reproduced the time-dependent concentration of RW in the arterial blood after a short-period inhalation of $^{15}O_2$ is indeed adequate. Our approach also simplified the procedures for sequential assessment of RW in $^{15}O_2$ inhalation PET studies, although previous approaches required frequent blood samples and centrifuges of each arterial blood sample. The present approach is an extension of a previous study by Iida *et al* (1993) and Huang *et al* (1991). It is essential if one intends to apply the rapid $^{15}O_2$ PET technique (Kudomi *et al*, 2005) to pharmacologic and physiologic stress studies on a wide range of species. Because the PET acquisition period can be prolonged >3 mins, statistical accuracy can be significantly improved as compared with Ohta *et al* (1992) and other researchers (Fujita *et al*, 1999; Vafaee and Gjedde, 2000; Okazawa *et al*, 2001*a*, *b*; Yamauchi *et al*, 2003; Mintun *et al*, 2002), under which to avoid effects of RW, the data acquisition period was limited only to <3 mins (Meyer *et al*, 1987; Ohta *et al*, 1992).

The present RW formula consists of three rate parameters of the production rate of RW in the arterial blood (k), and the forward and backward diffusion rate constants of RW between the blood and the peripheral tissues. The k was presumed to correspond to the oxygen metabolism in the total body system, $BMRO_2$, and was in fact shown to be

Table 2 Averaged values of k, Δt, k_w, and p for monkeys, pigs, rat, and human subjects under baseline condition

	Weight (kg)	k *(per min)*	*Δt (secs)*	k_w *(per min)*	p
Monkey	5.2 ± 0.8^a	0.34 ± 0.16^a	4.5 ± 1.4^a	0.98 ± 0.48	0.98 ± 0.30
Pig	38 ± 9^a	$0.11 \pm 0.02^{a,b}$	10.8 ± 1.8^a	0.83 ± 0.19	1.01 ± 0.26
Rat	0.30 ± 0.054^a	0.73 ± 0.16^a	2.9 ± 1.7^a	0.87 ± 0.30	0.83 ± 0.32
Human	58 ± 10^a	$0.129 \pm 0.023^{a,b}$	—	—	—

Monkey: $n = 6$; pig: $n = 3$; rat: $n = 12$; and human: $n = 231$. Measured values were obtained by 4PF for monkey, pig, rats, whereas those for human were obtained using data in a steady-state method.

[a]Denotes $P < 0.001$ for other species.

[b]Denotes that the difference was not significant in k between pig and human subjects.

Table 3 Values of k and $CMRO_2$ in the whole brain region for monkeys under physiologically baseline and stimulated conditions

ID	*Condition*	k *(per min)*			*$CMRO_2$ (mL/min per 100 g)*			
		4PF	*1PF*	*$BMRO_2$*	*Reference*	*4PF*	*1PF*	*$BMRO_2$*
1	BL	0.36	0.42	—	3.7	3.7	3.6	—
2	BL	0.62	0.66	1.24	3.0	3.3	3.4	3.4
3	BL	0.32	0.39	0.83	3.0	3.1	3.0	2.9
	(Dose of propofol)							
4	BL	0.21	0.18	0.55	2.0	2.0	2.0	1.8
	8 mg/kg/h	—	0.30	0.69	—	—	—	—
	12 mg/kg/h	—	0.23	0.52	—	—	—	—
	16 mg/kg/h	—	0.16	0.40	—	—	—	—
5	BL	0.12	0.15	0.31	2.1	2.1	2.0	1.8
	5 mg/kg/h	—	0.15	0.32	—	—	—	—
	7 mg/kg/h	—	0.16	0.35	—	—	—	—
	10 mg/kg/h	—	0.18	0.36	—	—	—	—
	15 mg/kg/h	—	0.071	0.29	—	—	—	—
	($PaCO_2$ level)							
6	BL	0.43	0.46	0.95	2.8	3.1	3.0	3.3
	47 mm Hg	—	0.20	0.64	—	—	—	—
	33 mm Hg	—	0.21	0.46	—	—	—	—
	26 mm Hg	—	0.14	0.28	—	—	—	—
	42 mm Hg	—	0.33	0.82	—	—	—	—

4PF, four parameters fitting; 1PF, one parameter fitting; $BMRO_2$, total body metabolic rate of oxygen; BL, baseline condition.
Reference: RW TAC was obtained using measured RW data at a baseline condition in all monkeys ($n = 6$). No statistically significant differences were found in $CMRO_2$ between reference and other techniques.

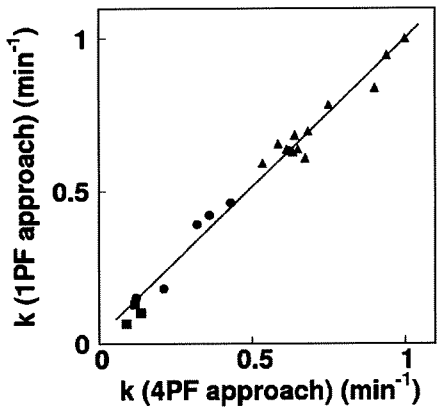

Figure 3 Comparison of the production rates of RW (k, per min) obtained by 4PF and those by 1PF. Squares, circles, and triangles correspond to pigs, monkeys, and rats, respectively. The regression line was $y = 0.97x + 0.026$ (per min) ($r = 0.98$).

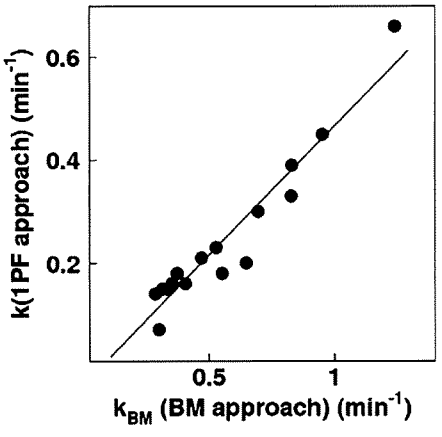

Figure 4 Comparison of the production rates of RW obtained by BM approach and those by 1PF approach in five monkeys at various anesthetic and $PaCO_2$ levels. The regression line was $y = 0.50x - 0.034$ (per min) ($r = 0.95$).

significantly correlated to $BMRO_2$, as measured from the trachea gas sampling (Figure 4). The latter two parameters (k_w and p) appeared to be consistent and did not differ across various species (Table 2). Also, change in those parameters was less sensitive in $CMRO_2$ (Figure 1). These findings suggest that the production of RW after inhalation of $^{15}O_2$ could be described only by a single parameter of k, as shown in Figure 3, although further studies are required to validate this because the method was only tested in a group with small number of subjects of particular physiologic situation (under anesthesia) and has not been applied to different populations. It is also important to note that this parameter (k) estimated from the $BMRO_2$ (i.e., BM approach) provided $CMRO_2$, which was consistent with the trachea gas samplings shown in Figure 4, and that the obtained OEF values by the approaches of 4PF, 1PF, and BM applied in the present study were not significantly different to that by A–V difference approach as revealed by Bland–Altman analysis.

The simulation study also showed that the most sensitive parameter in $CMRO_2$ was the RW production rate constant, k, followed by Δt. It was therefore suggested that k could be determined with a single blood sampling procedure using the 1PF approach, in which other parameter values were determined and fixed from results from the 4PF approach. It was further showed that k could be obtained from the BM approach as determined from oxygen concentration in the expiration gas. Both 1PF and BM approaches appeared to be robustly useful in $^{15}O_2$ PET for assessing quantitative $CMRO_2$ and CBF in clinical studies.

It is important to note that k varies significantly depending on the physiologic status even in the same species, as seen in Figure 4. According to the simulation study in Figure 1, this variation causes nonnegligible errors in $CMRO_2$, if a constant k is used. Changes in k from 0.1 to 0.6 per min causes errors in $CMRO_2$ of $\pm 30\%$ in anesthetized monkeys. Results from clinical studies, however, showed the variation in k being less. As shown in Table 2, k for clinical patients was 0.129 ± 0.023 per min, and the coefficient of variation was approximately 18%. Previous work by Huang *et al* (1991) also showed similar value with comparable variations, namely 0.131 ± 0.026 per min in six human subjects. These variations caused only $\pm 5\%$ errors in $CMRO_2$, according to the simulation shown in Figure 1. The small variation in k in clinical patients is attributed to the fact that all subjects were studied at a relatively stable condition without physiologic stimulation. However, careful attention is needed if one intends to scan the patients whose whole-body oxygen metabolism is largely changed from the baseline condition. For example, during several pharmacologically stressed (Wessen *et al*, 1997; Kaisti *et al*, 2003), exercise-induced physically stressed, and hyper- or hypothermia (Sakoh and Gjedde, 2003) conditions.

The simulation also showed that size of errors in $CMRO_2$ increased in smaller animals, where the value of k was larger. Recently, $CMRO_2$ as well as CBF have been measured in rats using a small animal PET scanner (Magata *et al*, 2003; Yee *et al*, 2006). Magata *et al* performed multiple blood samplings and plasma separation for multiple blood samples to estimate the RW in their experiment involving rats. The procedures were crucial, but have caused serious alterations of physiologic condition in heart pressure and heart rate due to large amount of blood samples for small animals. Our proposed simplified technique for estimating RW from a single blood sample or from $BMRO_2$, is essential for small animals to be able to maintain the physiologic status. The calculation of $CMRO_2$ also requires whole blood arterial TAC, which can be obtained from arterial blood samplings and could change the physiologic condition. However, such blood sampling could also be avoided by an arterial–venous bypass (Weber *et al*, 2002; Laforest *et al*, 2005), by placing a probe in femoral artery (Pain *et al*, 2004), or by a noninvasive method (Yee *et al*, 2006).

Mintun *et al* (1984) has proposed a simple procedure for RW correction based on a linear interpolation for the bolus $^{15}O_2$ inhalation 60-secs PET scan. As shown in Figure 2, the RW curve is not linear particularly in smaller animals, and a systematic error may be caused or scan duration is limited. Ohta *et al* (1992) and other investigators (Ohta *et al*, 1992; Fujita *et al*, 1999; Vafaee and Gjedde, 2000; Okazawa *et al*, 2001*a*, *b*; Yamauchi *et al*, 2003; Mintun *et al*, 2002), however, have used a technique which does not take into account the RW contribution. Only initial short-period data, namely the 3 mins after the bolus inhalation of $^{15}O_2$, were used in their approach, and thus estimated parameters suffered from statistical uncertainties. The present methodology to estimate RW in the arterial blood allows the prolongation of a PET acquisition period. The technique can also be applicable to the recently proposed sequential administration protocol of $^{15}O_2$ followed by $H_2^{15}O$ to estimate $CMRO_2$ and CBF simultaneously from a single session of a PET scan (Kudomi *et al*, 2005). This protocol, however, required a separation of a RW TAC from the whole blood TAC as showed recently (Kudomi *et al*, 2007).

The k_{BM} determined from the total body oxygen metabolism, namely the BM approach, was significantly greater than k obtained by the 4PF or the 1PF approach, by a factor 2, as shown in Figure 4. The reason is not clear, but partly attributed to the limitation of the simplified model. The body system consists of various organs which have different oxygen metabolism along with different circulation systems and with transit times. It is well known that the apparent rate constant defined with a simplified compartmental model could be underestimated as compared with an average of true rate constants, known as heterogeneity effects (Iida *et al*, 1989; Aston *et al*, 2002). This is, however, not essential.

Simply, linear correction could be applied to convert to the apparent k value as has been performed in this study. $CMRO_2$ values calculated using BM approach for the RW separation, were in good agreement with those determined with the direct measurement of RW as shown in Table 3.

The current method with modeling approach and simplified procedure provided consistent results in terms of time-dependent RW component, and consequently metabolic product of $^{15}O_2$ was separated from arterial whole blood for the $CMRO_2$ assessment in PET examination. The modeling approach to separate metabolite from authentic tracer has been showed previously for 6-[^{18}F]fluoro-L-dopa study (fdopa) (Huang *et al*, 1991). We expect that the modeling approach in conjunction with the simplified method showed in our study could be applied for various kinds of tracers, which require the separation of metabolic product such as fdopa. This approach enables us to assess parametric images for those tracers by eliminating the laborious procedures and by avoiding the amount of blood samplings, particularly for smaller animals.

In conclusion, the present RW model was feasible to reproduce RW TAC from a whole radioactivity concentration curve obtained after $^{15}O_2$ inhalation, and for a wide range of species. The simplified procedure to predict the RW TAC is of use to calculate $CMRO_2$ in smaller animals as well as clinical patients.

Acknowledgements

We acknowledge Mr N Ejima for operating the cyclotron and daily maintenance of CTI ECAT HR. We also gratefully thank Ms Atra Ardekani for her invaluable help on preparing the present paper. We also thank the staff of the Investigative Radiology, Research Institute, National Cardiovascular Center, especially, Dr T Inomata, Dr H Jino, Dr N Kawachi, and Dr T Zeniya for their assistance.

References

Aston JA, Cunningham VJ, Asselin MC, Hammers A, Evans AC, Gunn RN (2002) Positron emission tomography partial volume correction: estimation and algorithms. *J Cereb Blood Flow Metab* 22:1019–34

Eriksson L, Holte S, Bohm Chr, Kesselberg M, Hovander B (1988) Automated blood sampling system for positron emission tomography. *IEEE Trans Nucl Sci* 35:703–7

Eriksson L, Kanno I (1991) Blood sampling devices and measurements. *Med Prog Technol* 17:249–57

Fujita H, Kuwabara H, Reutens DC, Gjedde A (1999) Oxygen consumption of cerebral cortex fails to increase during continued vibrotactile stimulation. *J Cereb Blood Flow Metab* 19:266–71

Hayashi T, Watabe H, Kudomi N, Kim KM, Enmi J, Hayashida K, Iida H (2003) A theoretical model of oxygen delivery and metabolism for physiologic interpretation of quantitative cerebral blood flow and metabolic rate of oxygen. *J Cereb Blood Flow Metab* 23:1314–23

Hirano T, Minematsu K, Hasegawa Y, Tanaka Y, Hayashida K, Yamaguchi T (1994) Acetazolamide reactivity on ^{123}I-IMP single photon emission computed tomography in patients with major cerebral artery occlusive disease: correlation with positron emission tomography parameters. *J Cereb Blood Flow Metab* 14:763–70

Holden JE, Eriksson L, Roland PE, Stone-Elander S, Widen L, Kesselberg M (1988) Direct comparison of single-scan autoradiographic with multiple-scan least-squares fitting approaches to PET $CMRO_2$ estimation. *J Cereb Blood Flow Metab* 8:671–80

Huang SC, Barrio JR, Yu DC, Chen B, Grafton S, Melega WP, Hoffman JM, Satyamurthy N, Mazziotta JC, Phelps ME (1991) Modelling approach for separating blood time-activity curves in positron emission tomographic studies. *Phys Med Biol* 36:749–61

Iida H, Jones T, Miura S (1993) Modeling approach to eliminate the need to separate arterial plasma in oxygen-15 inhalation positron emission tomography. *J Nucl Med* 34:1333–40

Iida H, Kanno I, Miura S, Murakami M, Takahashi K, Uemura K (1989) A determination of the regional brain/blood partition coefficient of water using dynamic positron emission tomography. *J Cereb Blood Flow Metab* 9:874–85

Kaisti KK, Langsjo JW, Aalto S, Oikonen V, Sipila H, Teras M, Hinkka S, Metsahonkala L, Scheinin H (2003) Effects of sevoflurane, propofol, and adjunct nitrous oxide on regional cerebral blood flow, oxygen consumption, and blood volume in humans. *Anesthesiology* 99:603–13

Kudomi N, Choi C, Watabe H, Kim KM, Shidahara M, Ogawa M, Teramoto N, Sakamoto E, Iida H (2003) Development of a GSO detector assembly for a continuous blood sampling system. *IEEE Trans Nucl Sci* 50:70–3

Kudomi N, Hayashi T, Teramoto N, Watabe H, Kawachi N, Ohta Y, Kim KM, Iida H (2005) Rapid quantitative measurement of $CMRO_2$ and CBF by dual administration of ^{15}O-labeled oxygen and water during a single PET scan—a validation study and error analysis in anesthetized monkeys. *J Cereb Blood Flow Metab* 25:1209–24

Kudomi N, Watabe H, Hayashi T, Iida H (2007) Separation of input function for rapid measurement of quantitative $CMRO_2$ and CBF in a single PET scan with a dual tracer administration method. *Phys Med Biol* 52: 1893–908

Laforest R, Sharp TL, Engelbach JA, Fettig NM, Herrero P, Kim J, Lewis JS, Rowland DJ, Tai YC, Welch MJ (2005) Measurement of input functions in rodents: challenges and solutions. *Nucl Med Biol* 32:679–85

Lindstedt L, Schaeffer PJ (2002) Use of allometry in predicting anatomical and physiological parameters of mammals. *Lab Anim* 36:1–19

Magata Y, Temma T, Iida H, Ogawa M, Mukai T, Iida Y, Morimoto T, Konishi J, Saji H (2003) Development of injectable O-15 oxygen and estimation of rat OEF. *J Cereb Blood Flow Metab* 23:671–6

Meyer E, Tyler JL, Thompson CJ, Redies C, Diksic M, Hakim AM (1987) Estimation of cerebral oxygen utilization rate by single-bolus 15O2 inhalation and dynamic positron emission tomography. *J Cereb Blood Flow Metab* 7:403–14

Mintun MA, Raichle ME, Martin WR, Herscovitch P (1984) Brain oxygen utilization measured with O-15 radio-

tracers and positron emission tomography. *J Nucl Med* 25:177–87

Mintun MA, Vlassenko AG, Shulman GL, Snyder AZ (2002) Time-related increase of oxygen utilization in continuously activated human visual cortex. *Neuroimage* 16:531–7

Ohta S, Meyer E, Thompson CJ, Gjedde A (1992) Oxygen consumption of the living human brain measured after a single inhalation of positron emitting oxygen. *J Cereb Blood Flow Metab* 12:179–92

Okazawa H, Yamauchi H, Sugimoto K, Takahashi M, Toyoda H, Kishibe Y, Shio H (2001*a*) Quantitative comparison of the bolus and steady-state methods for measurement of cerebral perfusion and oxygen metabolism: positron emission tomography study using 15O-gas and water. *J Cereb Blood Flow Metab* 21:793–803

Okazawa H, Yamauchi H, Sugimoto K, Toyoda H, Kishibe Y, Takahashi M (2001*b*) Effects of acetazolamide on cerebral blood flow, blood volume, and oxygen metabolism: a positron emission tomography study with healthy volunteers. *J Cereb Blood Flow Metab* 21:1472–9

Pain F, Laniece P, Mastrippolito R, Gervais P, Hantraye P, Besret L (2004) Arterial input function measurement without blood sampling using a beta-microprobe in rats. *J Nucl Med* 45:1577–82

Sakoh M, Gjedde A (2003) Neuroprotection in hypothermia linked to redistribution of oxygen in brain. *Am J Physiol Heart Circ Physiol* 285:H17–25

Shidahara M, Watabe H, Kim KM, Oka H, Sago M, Hayashi T, Miyake Y, Ishida Y, Hayashida K, Nakamura T, Iida H (2002) Evaluation of a commercial PET tomograph-based system for the quantitative assessment of rCBF, rOEF and rCMRO2 by using sequential administration of 15O-labeled compounds. *Ann Nucl Med* 16:317–27

Temma T, Magata Y, Kuge Y, Shimonaka S, Sano K, Katada Y, Kawashima H, Mukai T, Watabe H, Iida H, Saji H (2006) Estimation of oxygen metabolism in a rat model of permanent ischemia using positron emission tomography with injectable ^{15}O-O_2. *J Cereb Blood Flow Metab* 26:1577–83

Vafaee MS, Gjedde A (2000) Model of blood-brain transfer of oxygen explains nonlinear flow-metabolism coupling during stimulation of visual cortex. *J Cereb Blood Flow Metab* 20:747–54

Votaw JR, Shulman SD (1998) Performance evaluation of the Pico-Count flow-through detector for use in cerebral blood flow PET studies. *J Nucl Med* 39:509–15

Weber B, Burger C, Biro P, Buck A (2002) A femoral arteriovenous shunt facilitates arterial whole blood sampling in animals. *Eur J Nucl Med Mol Imaging* 29: 319–23

Wessen A, Widman M, Andersson J, Hartvig P, Valind S, Hetta J, Langstrom B (1997) A positron emission tomography study of cerebral blood flow and oxygen metabolism in healthy male volunteers anaesthetized with eltanolone. *Acta Anaesthesiol Scand* 41:1204–12

Yamauchi H, Okazawa H, Kishibe Y, Sugimoto K, Takahashi M (2003) The effect of acetazolamide on the changes of cerebral blood flow and oxygen metabolism during visual stimulation. *Neuroimage* 20:543–9

Yee SH, Lee K, Jerabek PA, Fox PT (2006) Quantitative measurement of oxygen metabolic rate in the rat brain using microPET imaging of briefly inhaled 15O-labelled oxygen gas. *Nucl Med Commun* 27:573–81

Radiol Phys Technol
DOI 10.1007/s12194-008-0038-x

Use of a clinical MRI scanner for preclinical research on rats

Akihide Yamamoto · Hiroshi Sato · Jun-ichiro Enmi · Kenji Ishida · Takayuki Ose · Atsuomi Kimura · Hideaki Fujiwara · Hiroshi Watabe · Takuya Hayashi · Hidehiro Iida

Received: 27 May 2008 / Revised: 22 August 2008 / Accepted: 27 August 2008

Abstract This study evaluated the feasibility of imaging rat brains using a human whole-body 3-T magnetic resonance imaging (MRI) scanner with specially developed transmit-and-receive radiofrequency coils. The T_1- and T_2-weighted images obtained showed reasonable contrast. Acquired contrast-free time-of-flight magnetic resonance angiography images clearly showed the cortical middle cerebral artery (MCA) branches, and interhemispheric differences could be observed. Dynamic susceptibility contrast MRI at 1.17 mm^3 voxel resolution, performed three times following administration of gadolinium diethylenetriamine pentaacetic acid (Gd-DTPA, 0.1 mmol/kg), demonstrated that the arterial input function (AIF) can be obtained from the MCA region, yielding cerebral blood flow (CBF), cerebral blood volume, and mean transit time (MTT) maps. The hypothalamus (HT) to parietal cortex (Pt) CBF ratio was 45.11 ± 2.85%, and the MTT was 1.29 ± 0.40 s in the Pt region and 2.32 ± 0.17 s in the HT region. A single dose of Gd-DTPA enabled the assessment of AIF within MCA territory and of quantitative CBF in rats.

Keywords Quantitative mapping · Human whole-body 3-T MRI scanner · Single dose of Gd-DTPA · Dynamic susceptibility contrast (DSC) · Preclinical research · Rat brain

A. Yamamoto · J. Enmi · K. Ishida · T. Ose · H. Watabe · T. Hayashi · H. Iida (✉)
Department of Investigative Radiology,
Advanced Medical Engineering Center,
National Cardiovascular Center Research Institute,
5-7-1, Fujishiro-dai, Suita, Osaka 565-8565, Japan
e-mail: iida@ri.ncvc.go.jp

A. Yamamoto · A. Kimura · H. Fujiwara · H. Watabe · T. Hayashi · H. Iida
Department of Medical Physics and Engineering,
Division of Health Sciences, Graduate School of Medicine,
Osaka University, 1-7, Yamada-oka, Suita,
Osaka 565-0871, Japan

H. Sato
Laboratory for Diagnostic Solution,
Advanced Medical Engineering Center,
National Cardiovascular Center Research Institute,
5-7-1, Fujishiro-dai, Suita, Osaka 565-8565, Japan

1 Introduction

Magnetic resonance imaging (MRI) has been widely used in preclinical research on experimental small animals. Studies have typically been aimed at understanding the pathophysiologic status and evaluating the efficacy/side effects of newly developed treatments, such as pharmaceutical and regenerative medicine. Recently, a different idea has surfaced: the use of a human whole-body MRI scanner for small-animal imaging [1]. Although small-animal-dedicated scanners are superior to clinical scanners in terms of providing a better signal-to-noise ratio, the available pulse sequences are different from those in clinical scanners, and the magnetic field strength is often much higher. Small-animal imaging with clinical scanners is important for directly addressing clinical questions and/or identifying the origins of signal changes, including various disease conditions in a clinical setting.

Smith et al. [2] demonstrated that anatomic brain T_1- weighted (T_1W) images and T_2-weighted (T_2W) images can be obtained for healthy rats by using a 1-T clinical MRI scanner with a specially designed radiofrequency (RF) coil, given a reasonable spatial resolution (0.1953 × 0.1953 × 2.5 mm, 24 min of T_1W and 48 min of T_2W). The image contrast was sufficiently high to

distinguish the cortical gray matter from the white matter [corpus callosum (CC)], as well as the lateral ventricle (LV) and interpeduncular cistern (IPC) from the thalamus (Thal). Guzman et al. [3] employed a clinical 1.5-T MRI scanner with a commercially available RF coil and demonstrated that both T_1W and T_2W images can be obtained with good contrast, a reasonable spatial resolution of 0.3125 × 0.3125 × 1.5 mm, and an acquisition time of 19 min 51 s, as well as 0.35156 × 0.375 × 1.5 mm at 8 min 34 s, corresponding to T_1W and T_2W images, respectively. Other investigators [4] applied a clinical 1.5-T MRI scanner with a 3-in.-diameter circular receive-only surface coil to assess anatomic images. Their images can be used to evaluate the pathophysiologic status of stroke [4] and cancer [5, 6], as well as the effects of neural excitotoxicity [3]. There were also several studies that used a clinical 3-T MRI scanner fitted with commercial and/or hand-made RF coils to investigate the pathophysiology of stroke [7, 8] and brain tumors in rats [6, 9, 10]. Generally speaking, anatomic images with better contrast can be obtained in a stronger magnetic field, although there are additional factors that may influence the signal-to-noise ratio (SNR) or spatial resolution of anatomic images. Contrast-free time-of-flight magnetic-resonance angiography (TOF-MRA) can also be performed on rats; a reasonable spatial resolution was obtained by using a clinical 3-T MRI scanner with a single-turn solenoid coil [11].

Dynamic susceptibility contrast MRI (DSC-MRI) [12] has been widely used in clinical diagnosis, particularly in patients with stroke [13–19] and tumors [20]. The application of clinical MRI scanners has been extended to DSC-MRI studies of small animals with stroke [21, 22] and tumors [23] using a 1.5-T MRI scanner. Up to now, small-animal studies have been performed on 1.5-T MRI scanners only, and 3-T scanners have not been employed so far. This is largely attributed to the fact that the susceptibility-induced inhomogeneous magnetic field can cause more serious distortion of the images at a higher static magnetic field. In DSC-MRI studies, the echo planar imaging (EPI) technique is mainly used because fast acquisition is required for accurate tracking of the bolus passage of MR contrast agents. The EPI technique, however, is very sensitive to magnetic field inhomogeneity, and thus the EPI images of small-animal brains may be severely distorted. The gradient slew rate (SR) is not high enough to support a sufficiently short echo spacing period when clinical scanners are used for high spatial resolution imaging of small objects. Moreover, injected materials may cause further distortion [24]. The degree of distortion of dynamic EPI images of small-animal brains produced by a 3-T clinical scanner is currently unknown. The arterial input function (AIF) is also questionable. To the best of our knowledge, no DSC-MRI studies of small-animal brains on 3-T clinical scanners have been reported.

This study attempted to evaluate the feasibility of developing a human whole-body 3-T MRI system for small animals, particularly DSC-MRI with a single dose of gadolinium-diethylenetriamine pentaacetic acid (Gd-DTPA). The quality of various images—including the anatomic T_1W images, T_2W images, time-of-flight magnetic resonance angiography (TOF-MRA) images and DSC images—was tested, and the availability of the AIF obtained from rat brain was evaluated.

2 Materials and methods

2.1 Subjects

The subjects were three healthy adult rats supplied by Japan SLC, Inc. (Shizuoka, Japan). All three rats were males, and they ranged in age from 20 to 24 weeks. Their weight range was between 400 and 600 g. Anesthesia was administered with an intramuscular injection of ketamine (33 mg/kg; Daiichi-Sankyo Co., Ltd., Tokyo, Japan) and xylazine (6.6 mg/kg; Bayer Yakuhin, Ltd., Osaka, Japan). The first rat (Sprague Dawley, SD) was used for T_1-W and T_2W imaging of the whole brain. The second rat, also a SD, was used for contrast-free TOF-MRA imaging. The third was a Wistar rat, which was used for a Gd-DTPA (0.1 mmol/kg; Bayer Yakuhin, Ltd., Osaka, Japan)-enhanced DSC-MRI sequence. Experiments were carried out according to the protocol approved by the Local Committee for Laboratory Animal Welfare, National Cardiovascular Center, Osaka, Japan.

2.2 MRI acquisition

A human whole-body 3-T MRI scanner (Signa, GE Healthcare, Milwaukee, WI, USA) equipped with a 55-cm bore was employed in this study. The gradient coil system was capable of providing a maximum gradient amplitude of 40 mT/m and an SR of 150 T m^{-1} s^{-1}. All sequence programs employed in this study were designed for clinical studies.

Two solenoid coils designed for rats were specially developed to cover the whole brain, and were capable of both transmitting and receiving RF pulses. The three-turn solenoid coil, which had a diameter of 42 mm and a length along its cylindrical axis of 18 mm, was attached to an apparatus made from an acrylic mold, as shown in Fig. 1. All components of the stereotaxic apparatus consisted of nonmagnetic materials that fixed the head positions of the rats during data acquisition. The RF coil was designed to have an impedance of 50 Ω at a resonance frequency of

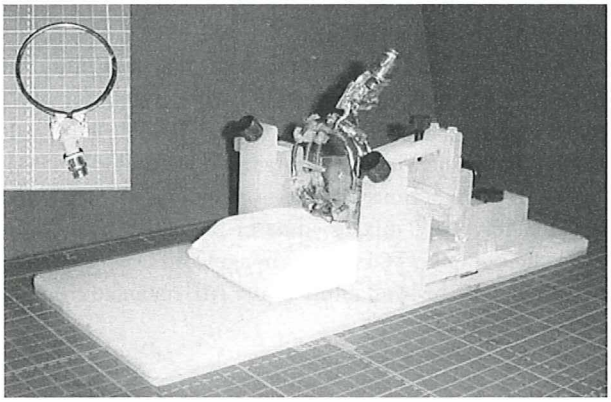

Fig. 1 The head fixation system for small animals, which was fitted with an MRI coil for RF transmission and reception. The coil is typically a three-turn solenoid; it can also be a single-turn coil, as shown on the *top left* of this figure

127.76 MHz. An additional single-turn surface coil of diameter 62 mm diameter was also developed for better homogeneity and was used for a single slice of DSC-MRI. The RF power in these coils had to be reduced to less than that used in the standard human head coil because of the diameter of the small coil. The transmission signal was therefore attenuated to 20 dB, which allowed the use of automated scanner software, including the calibration of the RF transmission power and receiver gains. All rats were fixed on the stereotaxic apparatus. They were placed at the center of the gantry and oriented with the craniocaudal axis perpendicular to the static magnetic field. Their heads were positioned inside the coil along the craniocaudal direction.

T_1W images were obtained with a conventional two-dimensional fast spin echo (2D-FSE) sequence. The repetition time (TR) was 1,500 ms [10]. The echo time (TE) was fixed at 14 ms. The echo train length (ETL) was 3. The field of view (FOV) was set at 40 × 30 mm^2, the slice thickness at 1.5 mm, the slice gap at 0.5 mm, the number of excitations (NEX) at 10, and the band width (BW) at 31.3 kHz. The acquired matrix (256 × 160) was interpolated, and null pixels were added in k-space to produce square matrices of 256 × 256. The acquisition time was 10 min 3 s.

T_2W images were obtained with a 2D-FSE and the following imaging parameters: TR, 4,100 ms; TE, 128 ms; ETL, 14; FOV, 40 × 30 mm; slice thickness, 1.5 mm; slice gap, 0.5 mm; NEX, 8; BW, 31.3 kHz; acquired matrix, 256 × 160, zero-filled to 256 × 256; phase direction, ventral-dorsal; acquisition time, 11 min 2 s.

Time-of-flight magnetic resonance angiography was performed using a three-dimensional flow-compensated spoiled gradient recalled (3D-SPGR) sequence prepared with magnetization transfer and with: TR, 53 ms; TE, 5.5 ms; flip angle (FA), 45°; BW, 16 kHz; FOV, 8 × 6 cm; slice thickness, 0.2 mm; one acquired slab of 512 × 512 × 64; voxel resolution, 0.156 × 0.156 × 0.2 mm^3; NEX, 1; acquisition time, 21 min 46 s.

Dynamic susceptibility contrast images were obtained following the intravenous administration of Gd-DTPA to the T_2*-weighted gradient echo dynamic images. A bolus of Gd-DTPA (0.1 mmol/kg) was injected manually into the tail vein with a 22-gauge catheter via 1 m of polyethylene tubing (PE50, internal diameter: 0.58 mm/outer diameter: 0.965 mm, Becton Dickinson and Company, Franklin Lakes, NJ, USA), and was followed by an additional administration of saline (1.0 ml). A multishot EPI (number of shots = 2) was employed to improve EPI distortion and temporal resolution. The imaging parameters were: TR, 142 ms; TE, 22.1 ms; FA, 20°; FOV, 40 × 40 mm; matrix size, 64 × 64, leading to a pixel size of 0.625 × 0.625 mm^2. The slice thickness was 3 mm in a single slice around the hypothalamus (HT). The temporal resolution was 0.284 s per image, and the acquisition time was 1 min 15 s. This assessment was repeated three times at intervals of 40 min and 10 min, corresponding to the first–second and second–third scans, respectively.

2.3 Data analysis

All MRI images were reconstructed on the same workstation provided for the GE Signa 3-T scanner used for the clinical programs. The images were then transferred to a Linux workstation. Lastly, data analysis was carried out using in-house and commercial software.

To evaluate the T_1W and T_2W image quality, we calculated the contrast-to-noise ratio (CNR) with an inter-tissue method [25–27] as follows: $CNR = (\pi/2)^{1/2} (SI_a - SI_b)/SI_{air}$, where SI_{air} represents the mean signal intensity of air, and SI_a and SI_b represent the signal intensities of tissue a and tissue b, respectively.

Angiograms were created by generating the partial maximum intensity projection (MIP) with commercial software [Virtual Place Liberty (VPL), AZE Co. Ltd., Tokyo, Japan]. Visible middle cerebral artery (MCA) branches and left-to-right differences in MCA were carefully investigated.

For the DSC images of slice sections containing the internal carotid artery (ICA) and/or MCA, a series of images were carefully observed. A region of interest (ROI) was carefully selected in the MCA region, from which the AIF was obtained, with the help of other anatomic information. To avoid susceptibility artifacts caused by air in the trachea, the area of the arterial circle of Willis was excluded from the definition of the AIF. The anterior cerebral artery was also excluded because of possible susceptibility effects attributed to venous blood. A Gaussian filter of full width at half maximum (FWHM) 1.1 mm

was applied to all dynamic images. The time versus signal intensity curves (TICs) were converted to the Gd-DTPA concentration according to Eq. 1 given in the "Appendix." Functional mapping images of the mean transit time (MTT), cerebral blood volume (CBV), and cerebral blood flow (CBF) were carried out with the deconvolution method [28]. The theory behind this is described in detail in the "Appendix." For ROI analysis, images of matrix size 64 × 64 were converted to 256 × 256 using a sinc interpolation function.

3 Results

T_1W and T_2W images reconstructed with a spatial resolution of 0.156 × 0.188 × 1.5 mm are shown in Fig. 2. White matter could be discriminated from cortical and deep gray matter regions. The locations of small anatomic features such as the caudate putamen (CPu), striatum, the CC, and the hippocampus (HC) could also be identified in both T_1W and T_2W anatomic images. The CNRs between the HC and CC were 15.6 and 9.8, respectively, for the T_1W and T_2W images shown in Fig. 2. The CNRs between the HC and IC were 23.2 and 13.6, respectively, although the CNR may be underestimated due to the contamination of signal from the globus pallidus.

Results for MIP images obtained with contrast-free TOF-MRA are shown in Fig. 3. Coronal MIP images around the HT of thickness 5 mm are shown in Fig. 3a. In this figure, the slice section contained ICAs and MCA. The MCA, the cortical branches in both the left and right hemispheres, can be identified. It is important to note that the anatomic structure of the cortical MCA arteries is different between the right and left hemispheres. The ROI for the AIF was selected in the MCA region and is shown by the arrows in Fig. 3a and b.

A typical example of a DSC-MRI image is shown in Fig. 4. Distortion of the DSC-MRI images is visible in Fig. 4A in the phase direction. A magnified area from dynamic images of the MCA region (shown as a rectangle in Fig. 4A) is displayed in Fig. 4B. Several pixels indicate temporal changes in pixel contrast as a function of time, and these are reflected by Gd-DTPA negative enhancement. The pixel signal intensity varied as shown in Fig. 4C, and the curve shown was employed to estimate the AIF. Figure 5 shows the TIC in this area together with the TIC for the whole brain region obtained from each of the three scans. The curves were visually reproducible in terms of the shapes, heights and widths of the curves around the peak, as well as the tail height at the end of the scan. It should also be noted that the baseline was consistent before each injection of Gd-DTPA, even though the second and

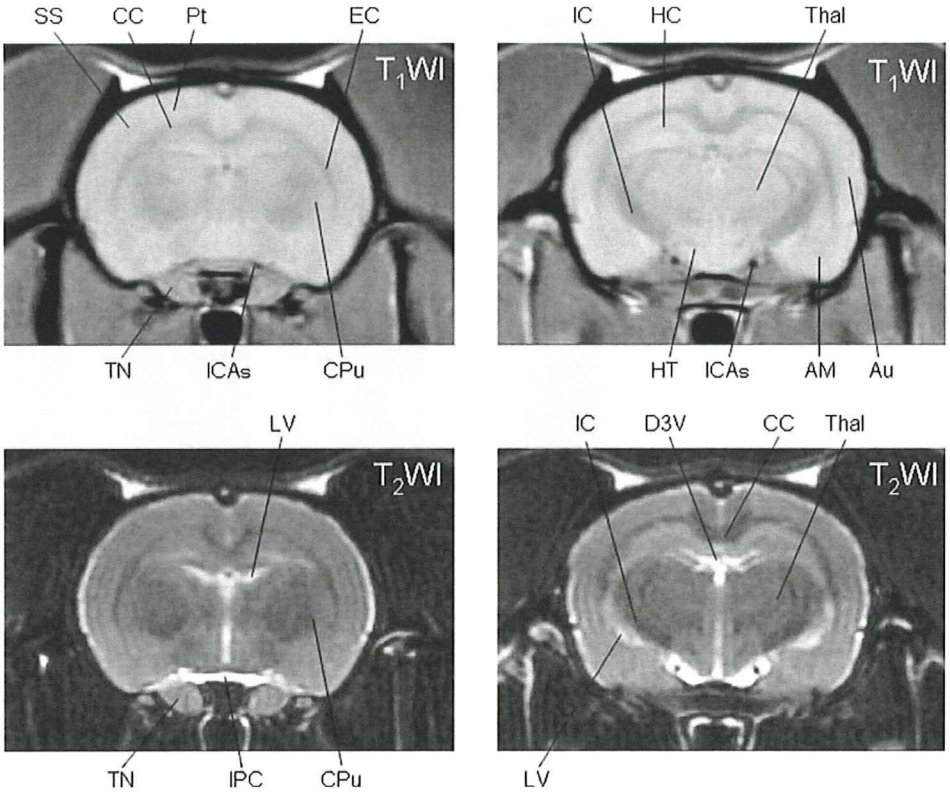

Fig. 2 T_1W images (*top*) and T_2W images (*bottom*) obtained from an SD rat, with the following anatomic locations as indicated: the somatosensory cortex (*SS*), corpus callosum (*CC*), parietal cortex (*Pt*), external capsule (*EC*), caudate putamen (*CPu*), internal capsule (*IC*), hippocampus (*HC*), thalamus (*Thal*), auditory cortex (*Au*), amygdala (*AM*), hypothalamus (*HT*), internal carotid arterial system (*ICAs*), trigeminal nerve (*TN*), interpeduncular cistern (*IPC*), dorsal third ventricle (*D3V*), and the lateral ventricle (*LV*). These slice sections were located −1.5 mm (*left*) and −3.5 mm (*right*), respectively, from the bregma